Composite CD-MOF nanocrystals-containing microspheres for sustained drug delivery

Haiyan Li[†‡], Nana Lv[†§‡], Xue Li[†×‡], Botao Liu[†¶], Jing Feng[†], Xiaohong Ren[†], Tao Guo[†], Dawei Chen[§], J. Fraser Stoddart[‡*], Ruxandra Gref[×*], Jiwen Zhang[†¶*]

[†] *Center for Drug Delivery System, Shanghai Institute of Materia Medica, Chinese Academy of Sciences, 501 Haike Road, Shanghai 201203, China*

[‡] *Department of Chemistry, Northwestern University, 2145 Sheridan Road, Evanston, IL 60208, USA*

[§] *School of Pharmacy, Shenyang Pharmaceutical University, 103 Wenhua Road, Shenyang 110016, China*

[×] *Institut des Sciences Moléculaires d'Orsay (ISMO), UMR CNRS 8214, Université Paris Sud,Université Paris-Saclay,Orsay 91400, France*

[¶] *School of Chemical and Environmental Engineering, Shanghai Institute of Technology, 500 Haiquan Road, Shanghai 201418, Chinar*

*E-mail: jwzhang@simm.ac.cn; ruxandra.gref@u-psud.fr; stoddart@northwestern.edu

---

Supporting Information

Table of Contents

1. Materials / General Methods / Instrumentation

γ-Cyclodextrin (γ-CD) was purchased from MaxDragon Biochem Ltd (China), ibuprofen (IBU) was obtained from Melonepharma Co Ltd and lansoprazole (LPZ) was provided by Zhuhai Rundu Co Ltd (China). Polyacrylic acid polymer (Eudragit RS 100) was provided by Evonik (Rohm Pharma GMBH, Darmstadt, Germany). Aluminum tristearate was purchased from Alfa Aesar (China). RPMI-1640 Medium was purchased from Corning Incorporated (Corning, NY, USA). Penicillin, streptomycin, acetic acid, polysorbate 80 (Tween 80) and dimethyl sulphoxide (Me_2SO) were obtained from Sigma-Aldrich (St Louis, MO, USA). Methanol (MeOH), potassium hydroxide (KOH), cetyl trimethyl ammonium bromide (CTAB), isopropanol (^iPrOH), ethanol (EtOH), acetone (Me_2CO), dichloromethane (CH_2Cl_2), acetic acid (HOAc) and other reagents of analytical grade were all purchased from Sinopharm Chemical Reagent Co Ltd (Shanghai, China) and used without further purification. Water was purified by Milli-Q system (Millipore). Morphological and size characterization of samples was conducted using a scanning electron microscope (S3400, Hitachi). The specimens were immobilised on a metal stub with double-sided adhesive tape and coated with gold, then observed under definite magnification. The size distributions of CD-MOF nanocrystals were also characterised by *in situ* measurements using Vasco Flex (Cordouan-tech, France) equipped with an in situ head, which is a flexible nanoparticle size analyser based on optical fiber dynamic light scattering. The crystallinity of the samples was characterized by powder X-ray diffractometric (PXRD) analysis. Diffraction patterns were detected with a Bruker D8 Advance diffractometer (Bruker, USA) of the locked coupled scan type. Samples were irradiated with monochromatised CuKα radiation and analysed over a 2θ angle range 3–40°. The PXRD pattern was collected with the tube voltage of 40 kV, and tube current of 40 mA and a scan speed of 0.1 s per step. Fourier-Transform Infrared

spectroscopy (FT-IR) spectra of samples were obtained using an FT-IR spectrometer (Nicolet Continuum XL, Thermo Fisher Scientific, USA). Briefly, the sample and KBr were mixed well in a ratio of 1:10, followed by compression to form a disk. 128 scans were carried out in wavenumber range 400–4000 cm^{-1} at a resolution of 4 cm^{-1}. Thermogravimetric analyses (TGA) were performed using a TGA/SDTA851 thermal analysis system (Mettler Toledo, Switzerland) at a heating rate of 10 °C·min^{-1} under an atmosphere of nitrogen. ^{1}H Nuclear magnetic resonance (^{1}H NMR) spectra were recorded at ambient temperature on a Bruker Avance 500 spectrometer, with a working frequency of 500 MHz for ^{1}H nuclei. A N_2 adsorption-desorption isotherm was measured using a liquid N_2 bath (−196 °C) and a porosimeter (TriStar 3000 V6.05 A, Micromeritics, USA). In order to remove interstitial solvents before measurement, the CD-MOF samples were activated by immersing them in CH_2Cl_2 for three days, dried under vacuum at 50 °C for 12 h and then at 50 °C for 6 h for outgassing. The drug loaded samples were dried under vacuum at 50 °C for 12 h and then at 50 °C for 6 h for outgassing without activation.

2. Synthetic Protocols

2.1 Preparation of Micron and Nanometer-Sized CD-MOFs

CD-MOFs were synthesised by solvent evaporation by employing an adaption of a published procedure.[S1] Compared with the published procedure at room temperature, higher temperature (50 °C) of MeOH diffusion was employed in this investigation. Noticeably, it was found that pre-addition of MeOH to the aqueous solution of γ-CD and KOH can shorten the synthesis time and improve the efficiency. Micron-sized CD-MOFs were prepared from a mixture of γ-CD (162 mg, 0.125 mmol) with 8 molar equiv of KOH (56 mg, 1 mmol) in H_2O (5 mL). The aqueous solution was filtered through a 0.45 μm filter membrane into a glass tube, and MeOH (0.5 mL) was added, followed by vapour diffusion of MeOH into the aqueous solution at 50 °C. After 6 h,

the supernatant was transferred into another glass tube with addition of CTAB (8 mg·mL^{-1}). After thoroughly dissolving CTAB, the aqueous solution was incubated overnight at room temperature. The precipitate was then harvested and washed with ^{i}PrOH three times, and dried (37 °C) overnight to produce CD-MOFs ca. 5–10 μm cubes (CD-MOF microcrystals). The synthetic procedure to produce nanometer-sized CD-MOFs (CD-MOF nanocrystals) was identical to that employed in the preparation of CD-MOF microcrystals, except that MeOH with the same volume of supernatant was added before CTAB was dissolved.

The stability of CD-MOF microcrystals was investigated by suspending CD-MOF microcrystals (500 mg) in different solvents (10 mL) at 70 °C, including EtOH, MeOH, Me_2CO, CH_2Cl_2, DMF and ^{i}PrOH. After 1 day, the crystallinity of CD-MOF crystals was characterised by PXRD. In addition, the release profile of CD molecules from CD-MOF microcrystals incubated in DMF was also measured. CD-MOF microcrystals (500 mg) were suspended in DMF (10 mL) at 70 °C. An aliquot (0.5 mL) of supernatant was subjected to analytical HPLC in order to quantify the released organic linker, γ-CD. The concentration of the released γ-CD in the supernatant was determined using the HPLC (Agilent 1290, USA) equipped with an evaporative light-scattering detector (ELSD). The analysis was carried out with the Diamonsil C18 column (4.6 mm×150 mm, 5 μm i.d.), under a flow rate of 1.0 mL·min^{-1} and an injection volume of 20 μL. The column temperature was kept at 25 °C. The mobile phase was composed of MeCN and H_2O (60:40). The ELSD detection was carried out with the drift tube temperature of 70 °C, the nebulizer gas pressure of 3.0 bar, and the photomultiplier of 1.0. The retention time for γ-CD occurred at about 2.5 min.

2.2 Encapsulation of Drugs in CD-MOFs

IBU and LPZ were used as model drugs. IBU- and LPZ-loaded CD-MOFs were prepared by

both impregnation and co-crystallisation techniques.

Impregnation Method. Impregnation was performed by soaking the dried CD-MOF powders in ethanolic solutions of the drugs. CD-MOFs (100 mg) soaked in an EtOH solution of IBU (40 mg·mL^{-1}, 2.5 mL) and CD-MOFs (200 mg) soaked in an EtOH solution of LPZ (14 mg·mL^{-1}, 3.6 mL) were incubated at 37 °C with a shaking speed of 100 rpm for an appropriate period of time. The drug-loaded CD-MOFs were collected by centrifugation and washed with the same incubation solvent three times (3×14 mL) until no drug molecules could be detected in the washing solution, ensuring any surface adsorbed free drug molecules were completely removed. After that, the sample was dried under vacuum overnight at 37 °C. In order to investigate the effect of solvents on drug loading, five solvents were selected as the incubation solvents namely EtOH, DMF, Me_2O, MeOH, and CH_2Cl_2. The drug concentrations were the same as those described above.

Co-crystallisation Method. The preparation of drug-loaded CD-MOFs by means of co-crystallisation was similar to that employed in the synthesis of CD-MOF nanocrystals, except that LPZ (30 mg·mL^{-1}) was added to the γ-CD-KOH solution initially, while IBU was dissolved in MeOH (20 mg·mL^{-1}) before CTAB was added. The effect of the drug concentration (20/30/40 mg·mL^{-1} for IBU and 10/20/30 mg·mL^{-1} for LPZ) on the drug loading was investigated.

2.3 Fabrication of CD-MOF/PAA Composite Microspheres

The CD-MOF/PAA composite microspheres were prepared by the solid in oil-in-oil (s/o/o) emulsifying solvent evaporation technique. Briefly, drug-loaded CD-MOF nanocrystals (50 mg) were uniformly dispersed in PAA Me_2CO solution (150 mg·mL^{-1}, 3 mL). A dispersion agent, aluminum tristearate (120 mg) was added to this solution and dispersed by sonication. The PAA solution containing aluminum tristearate and CD-MOF nanocrystals was poured into liquid

paraffin (20 mL) previously cooled at 10 °C. Then, the mixture was emulsified by Ultra-Turrax (IKA®, Germany) with a speed of 10,000 rpm for 5 min at 10 °C. The emulsion was heated to 35 °C gradually (heating rate of 1 °C·min^{-1}) and maintained at 35 °C for 3 h under stirring at 500 rpm to remove Me_2CO. The microspheres were collected by centrifugation, washed two times with n-hexane (25 mL each time) and dried under vacuum overnight.

For comparison, blank microspheres, IBU/LPZ microspheres and IBU/LPZ-γ-CD microspheres were also synthesised according to the emulsifying solvent evaporation procedure described above. The blank microspheres were prepared from PAA polymer. IBU/LPZ microspheres are obtained from drug raw materials and IBU/LPZ-γ-CD microspheres were synthesised from drug-γ-CD complexes (sieved with 200-mesh sieve). The drug-γ-CD complex was synthesised as follows. γ-CD (770 mg) was dissolved in the $NaHCO_3$-NaOH-buffered solution, $NaHCO_3$ (90 mg) was dissolved in H_2O (30 mL) and the pH was adjusted to 11 with 0.1 M NaOH solution while the temperature was maintained as 40 °C. The drug (220 mg for LPZ and 122 mg for IBU) was dissolved in EtOH (15 mL) so as to result in a molar ratio of drug to γ-CD of 1:1. The drug solution was added to γ-CD solution drop-by-drop while stirring for 2 h. EtOH in the resulting clear solution was removed by rotary evaporation at 45 °C for 40 min and the remaining liquid was dried under N_2 purging. The resulting residue was dried under vacuum at 35 °C overnight. The drug loadings of IBU-γ-CD and LPZ-γ-CD complexes were 11.2±0.44 and 19.6±0.31%, respectively.

In order to verify the presence of drug-loaded CD-MOF crystals in the microspheres, they were dissolved and CD-MOF crystals were isolated as follows. The microspheres (100 mg) were placed in a 10-mL Eppendorf tube and EtOH (8 mL) was added under sonication (10 min) to dissolve the PAA polymer. The suspension was centrifuged (12,000 rpm, 5min) and precipitates, which were composed of CD-MOF and aluminum tristearate crystals with different densities,

were isolated. They were further separated after being dispersed in CH_2Cl_2 (8 mL) and centrifuged (12,000 rpm, 5 min), resulting in CD-MOF crystals in the precipitate and aluminum stearate floating in the upper layer. The CD-MOF crystals in the precipitate were harvested and dried for observation by SEM.

Drug loading (DL) is defined as the percent of drug measured in the drug-loaded CD-MOF or CD-MOF/PAA microsphere samples and was calculated according to the following equation:

$$\text{DL}\,(\%) = \frac{\text{Amount of drug in CD-MOFs or microspheres}}{\text{Total amount of drug-loaded CD-MOFs or microspheres}} \times 100 \qquad \text{(S1)}$$

The DL values of encapsulated drugs in CD-MOFs were measured by dissolving the sample (10 mg) in H_2O (6 mL). The amounts of the drugs were analysed by HPLC (Agilent 1290, USA). For CD-MOF/PAA composite microspheres, the drug loading was determined by dissolving the microspheres (5 mg) in 67% MeOH (v/v, 3 mL) under sonication for 10 min and analysing the solution by HPLC, equipped with a diode array detector. The analysis was carried out using a Phenomenex C18 column (4.6 mm×150 mm, 5 μm) with a flow rate of 1.0 $mL \cdot min^{-1}$ and an injection volume of 20 μL. IBU was detected at 263 nm and the column temperature was set at 35 °C. The mobile phase was composed of NaOAc buffer solution and MeCN (40:60, v/v). The NaOAc buffer solution was obtained by dissolving NaOAc (6.13 g) in pure H_2O (750 mL) and adjusting the pH to 2.5 with glacial HOAc. For LPZ, the detection wavelength was set at 284 nm. The mobile phase was composed of MeOH, H_2O, TEA and H_3PO_4 (640:360:5:1.5, pH was adjusted to 7.3 with H_3PO_4). The column temperature was maintained at 40 °C.

2.4 In vitro Release of Drugs from Microspheres

Microspheres equivalent to 1 mg of IBU or LPZ were suspended in the release medium (50 mL) containing polysorbate 80 (0.02%, w/v) and the suspension was maintained at 37 °C with a stirring rate of 100 rpm. The release medium for IBU was PBS with pH 7.4, and that for LPZ

was a carbonate buffer solution with pH 9.7 because of the instability of LPZ at pH of 7.4. These release mediums were prepared according to Chinese Pharmacopeia 2010. Samples (1.0 mL) were withdrawn at regular time intervals (0.5, 1, 2, 4, 6, 8, 12, 24 and 48 h) and the same volume of fresh medium was added. The concentration of the drug in each sample was determined by the HPLC and the release percentage was calculated. Experiments were performed in triplicate.

2.5 Cytotoxicity Assays

The cytotoxicity of CD-MOF and CD-MOF/PAA composite microspheres was evaluated on J774 macrophage cells using the MTT (3-(4,5-dimethylthiazol-2-yl)-2,5-diphenyltetrazolium bromide) method. J774A.1 Cells (mouse macrophages, ATCC® TIB-67™) were grown in RMPI 1640 medium supplemented with 10% (v/v) fetal bovine serum (Gibco, USA), penicillin (100 $U \cdot mL^{-1}$) and streptomycin (100 $\mu g \cdot mL^{-1}$). Cells were maintained in a humidified incubator with 95% air and 5% CO_2 at 37 °C and seeded into 96-well microtiter plates at a density of 2000 $cells \cdot well^{-1}$. After incubating overnight, samples (20 μL) at concentrations equivalent to the IBU concentrations, ranging from 0.008 to 1.0 $mg \cdot mL^{-1}$ (with a five-fold dilution gradient) were added to the medium and incubated for 24 h. Then, MTT (15 μL, 5 $mg \cdot mL^{-1}$) was added to the cell culture medium and incubated for 4 h. Subsequently, the medium was replaced by Me_2SO (150 μL) to dissolve the insoluble crystals of formazan formed by living cells. The absorbance at 490 nm was read using a microplate reader (Multiskan GO, Thermo Fisher). Non-treated cells were used as a control and the cell viability (%) was calculated using Eq. S2. Results were expressed as mean ± standard deviation.

$$\text{Cell viability (\%)} = \frac{A_{490,\,\text{sample}}}{A_{490,\,\text{control}}} \times 100 \qquad \text{(S2)}$$

3. Data on Drug Encapsulation in MOF Particles[S2–S34]

Table S1 Overview of Drug Encapsulation in Metal-Organic Frameworks Particles

MOF	Metal Ion	Organic Linker	Inner Pore Size (Å)	Drug	Loading Method	Drug Loading (%, w/w)	Ref
MIL-100 (Cr)	Cr	BTC	25–29	Ibuprofen	Impregnation	25.9	S2
MIL-101 (Cr)	Cr	BDC	29–34	Ibuprofen	Impregnation	58	S2
MIL-53 (Cr) and MIL-53 (Fe)	Cr, Fe	BDC	8.6	Ibuprofen	Impregnation	20	S3
Bio-MOF-1	Zn	BPDC	5.2	Procainamide HCl	Cation exchange	18	S4
MIL-101 (Fe)	Fe	BDC	29–34	Ethoxysuccinato-cisplatin prodrug	Postsynthetic modification	12.8	S2, S5
MIL-101 (Cr)	Cr	BDC	29–34	Ibuprofen	Computational prediction	52.6	S2, S6
UMCM-1	Zn	BDC and H_3BTB	24–32	Ibuprofen	Computational prediction	57.6	S6
BioMIL-1	Fe	Nicotinic acid	–	Nicotinic acid	Active molecules as	71.5	S7
M-CPO-27	Co and Ni	2,5-Dihydroxyterephthalic acid	11–12	NO	Active molecules as	17.4	S8
NCP-1	Tb	Disuccinatocisplatin	–	Disuccinatocisplatin	Active molecules as	75	S9
$Ag_3(1)$	Ag	3-Phosphonobenzoic acid	–	Silver ions	Active molecules as	64.4	S10
$[(CH_3)_2NH_2]_2[Zn(TATAT)_{2/3}]$	Zn	5,5',5"-(1,3,5-Triazine-2,4,6-triyl)tris (azanediyl)triisophthalate	14.3–31.3	5-FU	Impregnation	33.3	S11
HKUST-1	Cu	BTC	6–12	Nimesulide	Impregnation	16.7	S12

MOF	Metal Ion	Organic Linker	Inner Pore Size (Å)	Drug	Loading Method	Drug Loading (%, w/w)	Ref
MIL-100 (Cr)	Cr	BTC	25–29	Peptides	Incubation	9–15	S13
MIL-101 (Cr)	Cr	BDC	29–34	Peptides	Incubation	20–39	S13
MIL-53 (Al)	Al	BDC	8.6	Peptides	Incubation	19–35	S13
MIL-100 (Fe)	Fe	BTC	25–29	Busulfan	Impregnation	26±3	S14
MIL-53 (Fe)	Fe	BDC	8.6	Busulfan	Impregnation	10±2	S14
MIL-88A (Fe)	Fe	Fumaric acid	6	Busulfan	Impregnation	8±1	S14
MIL-89 (Fe)	Fe	Muconic acid	11	Busulfan	Impregnation	14±2	S14
MOP-15	Cu	5-NH_2-*m*-Benzenedicarboxylate	16	5-FU	Impregnation	23.76	S15
Rho-ZMOF	In	4,5-Imidazoledicarboxylic acid	18.2	Procainamide HCl	Impregnation	9.9	S16
MIL-88B (Fe)	Fe	Terephthalate organic linkers bearing different functional groups	8	Caffeine	Impregnation	9.8–22.8	S17
$[Zn(BDC)(H_2O)_2]_n$	Zn	BDC	7	Ibuprofen	Impregnation	44.5	S18
IFMC-1	Zn	4,5-Di(1H-tetrazol-5-yl)-2H-1,2,3-triazole	11.6	5-FU	Impregnation	30.48	S19
Cu-BTC	Cu	BTC	9	5-FU	Impregnation	45.0	S20
CPO-27-Ni	Ni	2,5-Dihydroxyterephthalic acid	11–12	NO	Impregnation	15.3	S21
MIL-100 (Fe)	Fe	BTC	25–29	Caffeine	Impregnation	49.5±1.9	S22

MOF	Metal Ion	Organic Linker	Inner Pore Size (Å)	Drug	Loading Method	Drug Loading (%, w/w)	Ref
MIL-53 (Fe)	Fe	BDC	8.6	Caffeine	Impregnation	29.2±1.5	S22
UiO-66 (Zr)	Zr	BDC	8–11	Caffeine	Impregnation	22.4±3.4	S22
MIL-101 (Cr)	Cr	BDC	29–34	Naproxen	Incubation	–	S23
MOF-74-Fe (II)	Fe	2,5-Dioxido-1,4-benzenedicarboxylate	10.8	Ibuprofen	Ion exchange and salt	15.5	S24
UiO-66 (Zr)	Zr	BDC	8–11	Caffeine and Ibuprofen	Impregnation	20.4 and 20.7	S22, S25
Gd-pDBI	Gd	1,4-Bis(5-carboxy-1H-benzimidazole-2-yl)benzene	12–19	Doxorubicin	Sonication and stirring	12	S26
UiO-NMOFs	Zr	Aminotriphenyldicarboxylic acid	–	Cisplatin prodrug; Pooled SiRNAs	Post-synthetic encapsulation;	12.3±1.2; 81.6±0.6	S27
MIL-100 (Fe)	Fe	BTC	25–29	Topotecan	Impregnation	33	S28
CD-MOF-2	Rb	γ-CD	17	Rhodamine B	Co-crystallization	–	S29
MIL-100 (Al)	Al	BTC	25–29	Pd nanoparticles	Chemical wetting	10	S30
MIL-100 (Fe)	Fe	BTC	25–29	Azidothymidine-triphosphate	Impregnation	36.0	S31
MIL-100 (Fe)	Fe	BTC	25–29	Phosphorylated Azidothymidine	Impregnation	24.4±0.9	S32
MIL-100 (Fe)	Fe	BTC	25–29	Doxorubicin	Impregnation	30.7±0.8	S33
MIL-100 (Fe)	Fe	BTC	25–29	Phosphated gemcitabin	Impregnation	9.0	S34
CD-MOF-1	K	γ-CD	17	Ibuprofen Lansoprazole	Cocrystallsiation	12.7 4.5	This study

BTC: 1,3,5-Benzene tricarboxylic acid; BDC: 1,4-Benzenedicarboxylic acid; BPDC: Adenine and biphenyldicarboxylate; H_3BTB: 1,3,5-Tris(4-carboxyphenyl)benzene

4. Residual of CTAB, Stability and Size Distribution of CD-MOFs

As described in the Section 2.1 on the "Preparation of Micron and Nanometer-Sized CD-MOFs", the freshly obtained CD-MOF microcrystals and nanocrystals were washed with ^{i}PrOH three times, and dried (37 °C) overnight for further use. The ^{1}H NMR spectrum (**Fig. S1**) shows that there is no CTAB trapped in the CD-MOF nanocrystal after washing the CD-MOF nanocrystals with ^{i}PrOH three times. In addition, MeOH (δ = 3.34 ppm) was completely removed after the CD-MOF nanocrystals had been dried (37 °C) overnight.

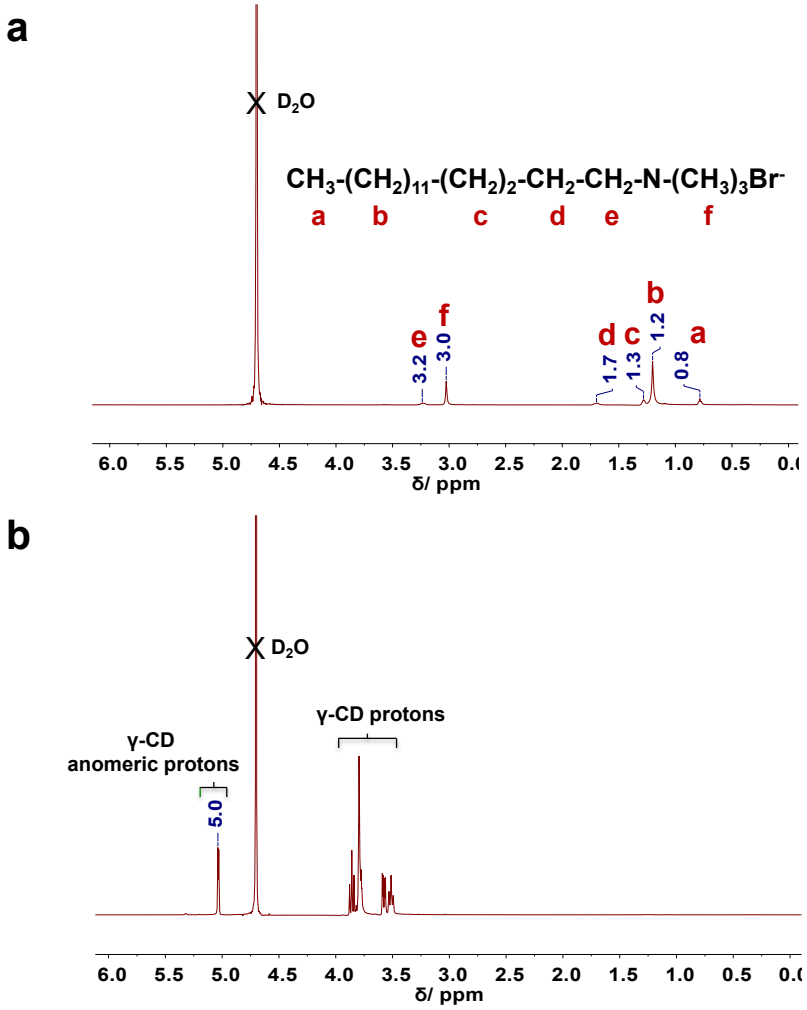

Fig. S1 ^{1}H NMR spectrum (500 MHz) in D_2O of a) CTAB (5 mg·mL^{-1}) and b) redissolved CD-MOF nanocrystals prepared from potassium hydroxide and γ-CD (10 mg·mL^{-1}), referenced to the H_2O peak (δ = 4.79 ppm).

The crystallinity of CD-MOFs decreases (**Fig. S2**) after one day of incubation with DMF, MeOH, Me_2CO and EtOH at 70 °C. In the case of DMF and MeOH, the intensity for all of the peaks decreased significantly and peaks at 16.7° disappeared, indicating the instability of CD-MOF microcrystals in DMF and MeOH. This observation might be a result of the relatively higher solubility of γ-CD in these two solvents. **Fig. S2** also illustrates the CD release profile for the CD-MOF microcrystals incubated in DMF at 70 °C for three days. It should be noted that about 4% of the total amount of the organic linker in the CD-MOF microcrystals was released after one day of incubation and 6% after three days of incubation.

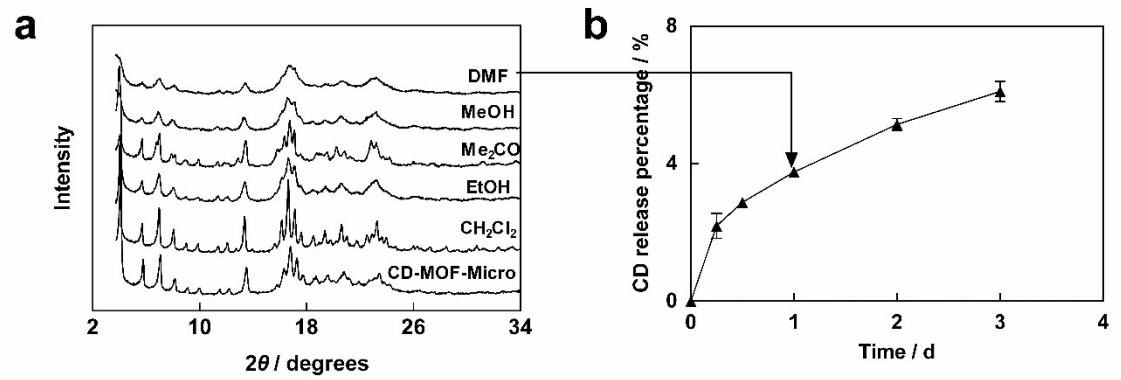

Fig. S2 a) PXRD Pattern of CD-MOF microcrystals incubated in different solvents at 70 °C for one day. b) The CD release profile for the incubation in DMF at 70 °C for three days. Error bars are based on repeating experiments on three batches of crystals.

The crystal size distributions of CD-MOF nanocrystals were characterised employing both SEM and DLS techniques. The SEM images (**Fig. 2b**) show the CD-MOF nanocrystals with diameters of 500–700 nm. The DLS result (**Fig. S3**) also reveals a mean diameter of 650 nm, with a polydispersity index of 0.22.

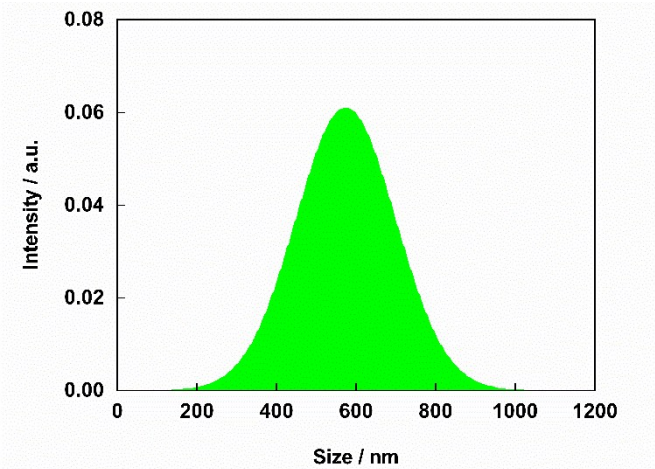

Fig. S3 Intensity particle size distribution of CD-MOF nanocrystals

5. Characterisation of Drug-Loaded CD-MOF Nanocrystals

The amount of drug-loaded into CD-MOFs of micron and nanometer sizes by impregnation and co-crystallisation methods are listed in **Table S2**. It is evident that IBU loading into CD-MOF microcrystals decreased from 12.0 to 6.6% compared with that obtained by the impregnation method. The LPZ loading in CD-MOF microcrystals however, increased from 9.4 to 16.6%, when the impregnation method was replaced by the co-crystallisation technique. In the case of the CD-MOF nanocrystals used to prepare microspheres, drug loading by the co-crystallisation was equivalent to or higher than that by the impregnation method.

Table S2 Drug loading by the impregnation (in EtOH) and the co-crystallisation method for micron and nanometer-sized CD-MOFs

Drug	CD-MOFs	DL (%, w/w) [c]	
		Impregnation	Co-crystallization
IBU	Micro[a]	12.0±0.7	6.6±0.4
	Nano[b]	13.0±0.2	12.7±0.6
LPZ	Micro[a]	9.4±0.3	16.6±0.4
	Nano[b]	1.6±0.1	4.5±0.3

[a] Micro indicates CD-MOF microcrystals with the size of 5–10 μm; [b] Nano indicates CD-MOF nanocrystals with the size of 500–700 nm; [c] DL values are based on repeating experiments on three batches of crystals.

Combined with HPLC analysis, ^{1}H NMR spectroscopy was also employed to estimate the amount of the drug within the CD-MOF nanocrystals prepared by co-crystallisation (**Fig. S4**). When the integral for the anomeric protons (δ ~ 5 ppm) of the γ-CD units is set to 8, representing one γ-CD torus, the aromatic proton signals of IBU (δ ~ 7 ppm) have a combined integral of 4.66 (**Fig. S4a**, four aromatic protons in each IBU molecule). This integral represents a molar ratio of 4:4.66 between γ-CD and IBU, corresponding to the IBU loading percentage of 14.6% (w/w) in IBU-loaded CD-MOF nanocrystals, a result which is similar with that of 12.6% (w/w) measured by HPLC. For LPZ (**Fig. S4b**), when integrating anomeric protons (δ ~ 5 ppm) of the γ-CD units and the pyridine-proton signal of LPZ (δ ~ 8 ppm), a molar ratio of 1:0.18 between γ-CD and LPZ is obtained, corresponding to the LPZ loading percentage of 4.5% (w/w) in LPZ-loaded CD-MOF nanocrystals, which is similar to that of 4.5% (w/w) measured by HPLC.

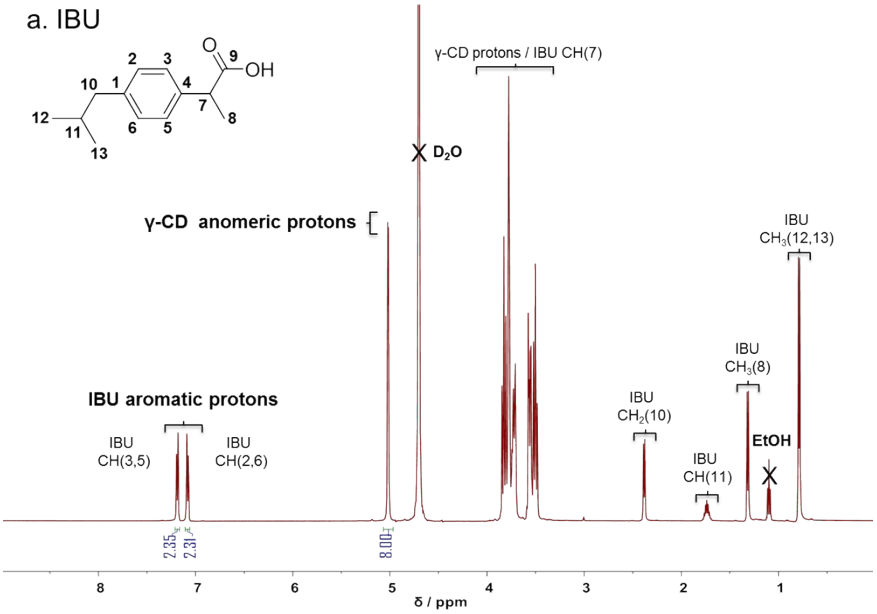

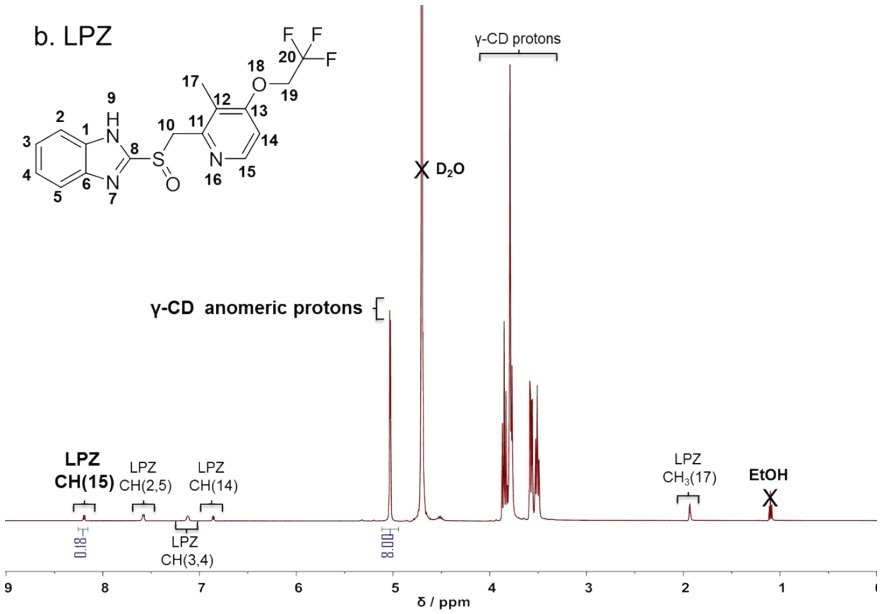

Fig. S4 ^{1}H NMR spectrum (500 MHz) in D_2O of drug-loaded CD-MOF nanocrystals prepared by co-crystallisation (10 mg·mL^{-1}). a) IBU and b) LPZ.

From the SEM images (**Fig. S5**) of the drug-loaded CD-MOFs, it can be concluded that the size of the drug-loaded CD-MOF nanoparticles is about 500–700 nm. The crystallinity of the drug-loaded CD-MOFs, produced by the co-crystallisation technique, was retained as shown by the identical PXRD features mentioned in the main text. In the case of IBU/LPZ loading by impregnation, however the crystallinity of the CD-MOFs was altered as a consequence of the progressive degradation of the MOFs in the solvents.

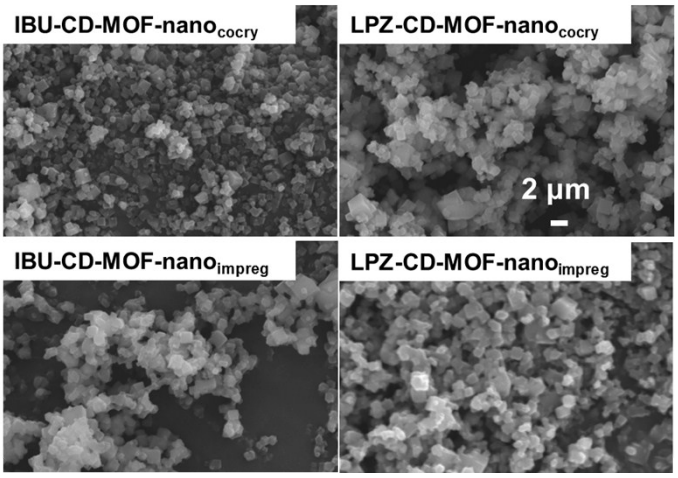

Fig. S5 SEM images of drug-loaded CD-MOF nanocrystals prepared by co-crystallisation and impregnation techniques.

Fig. S6 displays the IR spectra of the drug-loaded CD-MOFs. The characteristic vibrational band of the carboxylic group (ν(C=O)) in IBU, located at 1722 cm^{-1}, cannot be identified in the IBU-loaded CD-MOF nanocrystals. The ν(C=O) band is present, however, in a physical mixture with equivalent composition at 1722 cm^{-1}, indicating that the IR spectrum of IBU-loaded CD-MOF nanocrystals is different from that of the corresponding physical mixture. For LPZ, the characteristic vibrational band for the aromatic ring located at 1580 cm^{-1} also disappeared in the LPZ-loaded CD-MOF nanocrystals. In a physical mixture with an equivalent composition (LPZ loading of 4.5%), the characteristic vibrational band of the aromatic ring in LPZ at 1580 cm^{-1} was not detected as a consequence of the relative low loading of the drug (< 5%).

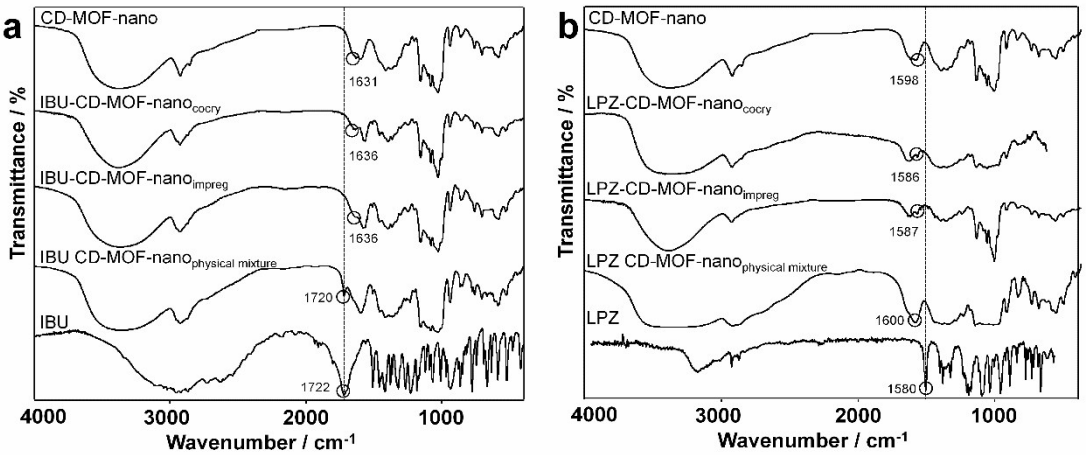

Fig. S6 IR Spectra of drug-loaded CD-MOF nanocrystals prepared by the co-crystallisation and impregnation techniques. a) IBU. b) LPZ.

TGA analysis was also used to confirm the incorporation of IBU into CD-MOF framework together with IR analysis (**Fig. S7**). After solvent loss below 100 ºC, the decomposition temperature is approximately 150 ºC for pure IBU and 175 ºC for CD-MOF. For the physical mixture of IBU and CD-MOF (87:13, w/w), the weight loss of about 14% (w/w) is found at 150–275 ºC, which can be identified as the IBU content. For IBU-loaded CD-MOF nanocrystals, however, weight loss does not appear until 200 ºC.

For LPZ, decomposition is observed at approximately 170 ºC, and the weight loss curve of LPZ-loaded CD-MOF nanocrystals almost overlaps with that of pure CD-MOF nanocrystals, an observation which is most likely a result of the relatively low drug loading percentage (4.5%).

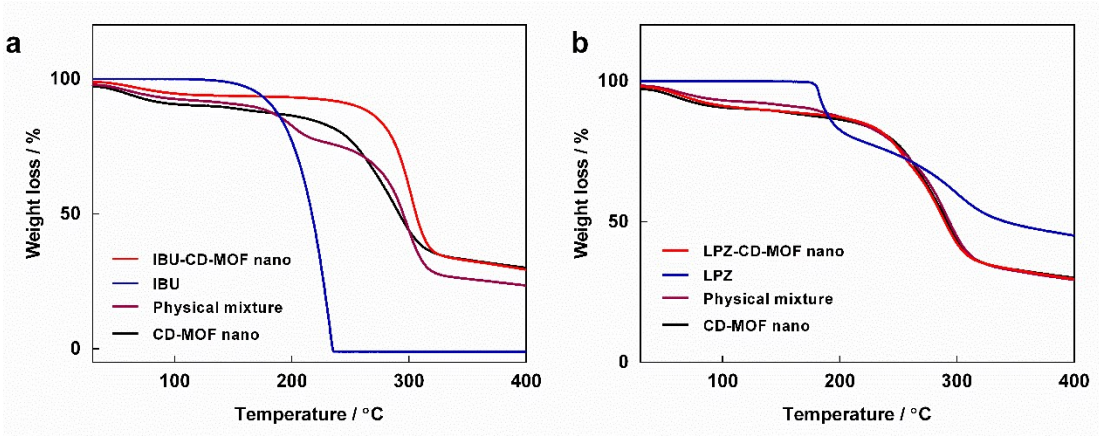

Fig. S7 TGA traces of drug-loaded CD-MOF nanocrystals prepared by the co-crystallisation. a) IBU. b) LPZ.

The BET surface area of CD-MOF materials was determined by N_2 adsorption using BET method. **Fig. S8** shows the nitrogen isotherms for CD-MOF microcrystals, CD-MOF nanocrystals and the drug-containing samples. The isotherms for CD-MOF crystals show the characteristic of the microporosities with a steep N_2 uptake in the low-pressure regions (P/P_0<0.05). The BET surface areas are 1002, 786, 668, 96 and 158 $m^2 \cdot g^{-1}$ for CD-MOF (100-micron meter), CD-MOF microcrystals, CD-MOF nanocrystals, IBU-loaded and LPZ-loaded CD-MOF nanocrystals, respectively (**Table S3**). The surface areas of CD-MOF micron and nanocrystals are decreased compared with that of the CD-MOF (100-micron meter). This observation might be as a result of the size reduction[S35], and the trace amount of CTAB residue in the sample, which is under the detection limit of ^{1}H NMR spectroscopy and might block partially the pores of CD-MOF. After drug incorporation, the BET surface area of the CD-MOF nanocrystals decreases dramatically,

indicating the drug fills completely and/or blocks the pores of the material leaving little to no accessible pore volume for nitrogen.[S2]

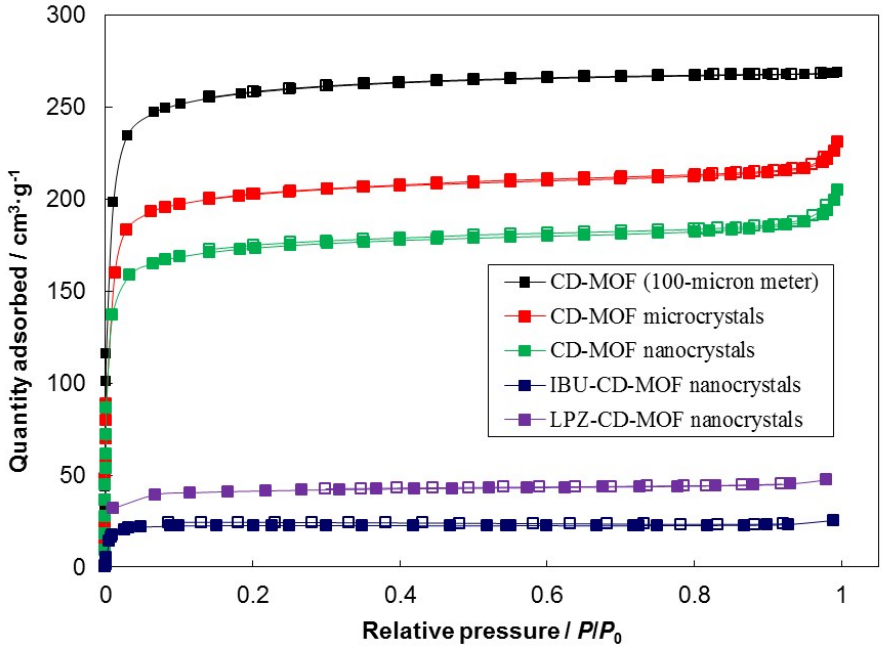

Fig. S8 N_2 Adsorption-desorption isotherms measured at 77 K for activated samples of CD-MOF microcrystals, CD-MOF nanocrystals and drug-loaded CD-MOF nanocrystals prepared by co-crystallisation. Filled and open symbols represent adsorption and desorption curves, respectively.

Table S3 The surface area of CD-MOFs and drug-loaded CD-MOF nanocrystals

	Surface area ($m^2 \cdot g^{-1}$)		
	S_{BET}	S_{micro}	$S_{external}$
CD-MOF (100-micron meter)	1002	950	52
CD-MOF microcrystals	786	754	32
CD-MOF nanocrystals	668	625	43
IBU-CD-MOF nanocrystals	96	88	8
LPZ-CD-MOF nanocrystals	158	133	24

S_{BET}: BET surface area; S_{micro}: micropore surface area; $S_{external}$: external surface area; The micropore surface area and the external surface area are calculated by the *t*-plot method.

6. Characterisation and Drug Release of the Composite Microspheres

In order to verify the presence of the drug-loaded CD-MOF crystals in the microspheres, samples were treated with EtOH and CH_2Cl_2 so as to remove and separate PAA and aluminum tristearate crystals from the CD-MOFs. The SEM images (**Fig. S9**) of the

retrieved CD-MOFs verify the intact morphology of the drug-loaded CD-MOFs crystals in the microspheres.

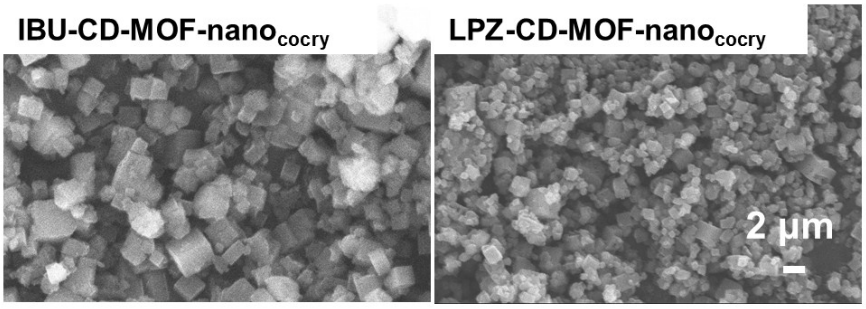

Fig. S9 SEM Images of the drug-loaded CD-MOF nanocrystals encapsulated in PAA composite microspheres after dissolving the microspheres with EtOH and removal of aluminum stearate.

For the drug loading of microspheres shown in **Table S4**, most of the values were consistent with the theoretical values, except for the microspheres prepared by IBU raw materials. The measured DL values were relatively higher than the theoretically calculated ones, an observation which might result from the adhesion of PAA on the side of the beaker and loss of PAA during microsphere preparation.

Table S4 Drug loading of microspheres prepared by drug raw material, drug-γ-CD complex and drug-loaded CD-MOF nanocrystals

Drug	DL (%, w/w) [a]		
	Drug microspheres	Drug-γ-CD microspheres	Drug-loaded CD-MOF microspheres
IBU	2.63±0.01 (8.06)	0.82±0.00 (0.90)	1.18±0.02 (1.02)
LPZ	9.85±0.21 (8.06)	1.52±0.03 (1.58)	0.59±0.00 (0.36)

a Values are based on repeating experiments on three batches of crystals and values in the parentheses represent the theoretical drug loading percentages. The components for all of the microspheres are drug or drug-γ-CD complex or drug-loaded CD-MOF (8.06%, w/w), PAA (72.58%, w/w) and aluminum tristearate (19.35%, w/w).

In the FT-IR spectrum (**Fig. S10**) of blank PAA microspheres , the sharp peaks at 2800–3000, 1600–1800 and 800–900 cm^{-1} can be assigned to the characteristic stretching

vibrations of C–H, C=O and C–O bonds in PAA. Compared with blank microspheres, the changes in these three characteristic peaks are observed in LPZ-CD-MOF/PAA composite microspheres and also in the LPZ and LPZ-CD microspheres. Especially in the case of the LPZ-CD-MOF/PAA composite microspheres, these peaks disappear or are broadened, indicating the strong interactions between the two components – namely, CD-MOFs and PAA – in the composite microspheres. In the case of the microspheres loaded with IBU, there is no significant change in the main characteristic peaks compared with those of the blank microspheres.

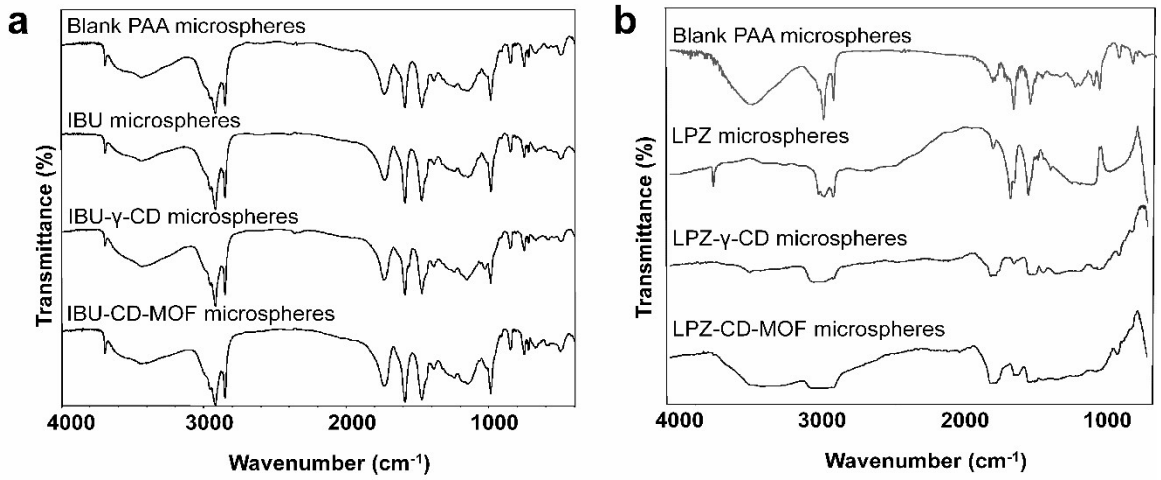

Fig. S10 IR Spectra of blank PAA microspheres, drug microspheres, drug-γ-CD microspheres and drug-loaded CD-MOF microspheres. a) IBU. b) LPZ.

Fig. S11 shows the release profiles of microspheres within the first 6 h, exhibiting the drug release behaviour in the initial stages. Microspheres containing drug-γ-CD complexes showed a very fast "burst" and uncontrolled release, i.e., 70% in 30 min, 80% in 2 h for both of the microspheres prepared from IBU and LPZ-γ-CD complexes. When drug-loaded CD-MOF nanocrystals were incorporated into the composite microspheres, steady and slow drug release was achieved, with release percentages being not more than

20% at 6 h: no burst release was observed.

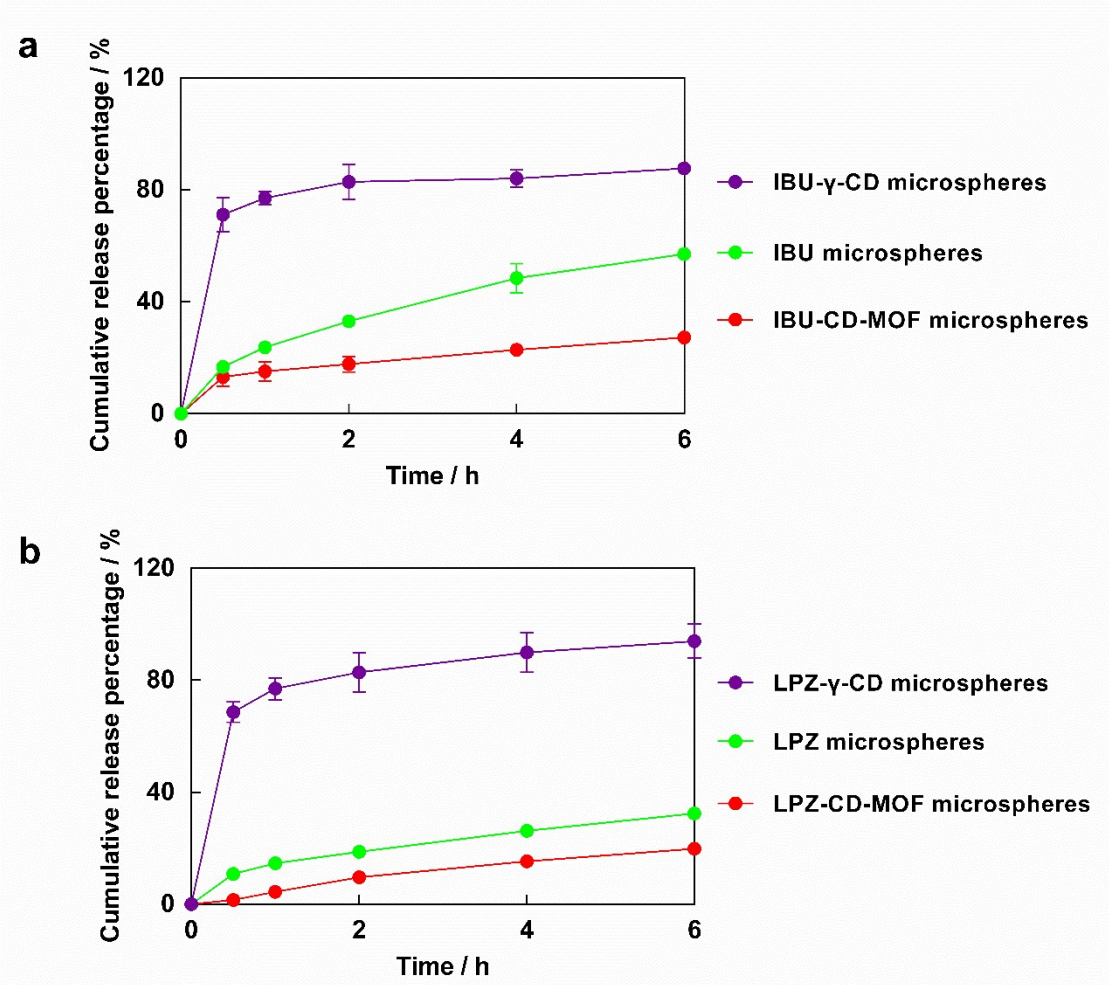

Fig. S11 The release profiles drug microspheres, drug-γ-CD microspheres and drug-CD-MOF microspheres. a) IBU. b) LPZ. Error bars are based on repeating experiments on three batches of microspheres.

7. References

S1 R. A. Smaldone, R. S. Forgan, H. Furukawa, J. J. Gassensmith, A. M. Slawin, O. M. Yaghi and J. F. Stoddart, *Angew. Chem. Int. Ed.*, 2010, **49**, 8630-8634. (b) Y. Furukawa, T. Ishiwata, K. Sugikawa, K. Kokado and K. Sada, *Angew. Chem. Int. Ed.*, 2012, **51**, 10566-10569.

S2 (a) P. Horcajada, C. Serre, M. Vallet-Regí, M. Sebban, F. Taulelle and G. Férey, *Angew. Chem. Int. Ed.*, 2006, **45**, 5974-5978. (b) N. Lv, T. Guo, B. T. Liu, C. F. Wang, V. Singh, X. N. Xu, X. Li, D. W. Chen, R. Gref and J. W. Zhang, *Pharm. Res.*, 2016, Epub ahead of print.

S3 P. Horcajada. C. Serre, G. Maurin, N. A. Ramsahye, F. Balas, M. Vallet-Regí, M. Sebban, F. Taulelle and G. Férey, *J. Am. Chem. Soc.*, 2008, **130**, 6774-6780.

S4 (a) J. An, S. J. Geib and N. L. Rosi, *J. Am. Chem. Soc.*, 2009, **131**, 8376-8377. (b) J. An and N. L. Rosi, *J. Am. Chem. Soc.*, 2010, **132**, 5578-5579.

S5 K. M. Taylor-Pashow, Rocca. J. Della, Z. Xie, S. Tran and W. Lin, *J. Am. Chem. Soc.*, 2009, **131**, 14261-14263.

S6 (a) K. Koh, A. G. Wong-Foy and A. J. Matzger, *Angew. Chem. Int. Ed.*, 2008, **47**, 677-680. (b) R. Babarao and J. Jiang, *J. Phys. Chem. C*, 2009, **113**, 18287-18291.

S7 S. R. Miller, D. Heurtaux, T. Baati, P. Horcajada, J. M. Grenèche and C. Serre, *Chem. Commun.*, 2010, **46**, 4526-4528.

S8 N. J. Hinks, A. C. Mckinlay, B. Xiao, P. S. Wheatley and R. E. Morris, *Micropor. Mesopor. Mat.*, 2010, **129**, 330-334.

S9 R. C. Huxford, Rocca. J. Della and W. Lin, *Curr. Opin. Chem. Biol.*, 2010, **14**, 262-268.

S10 M. Berchel, T. L. Gall, C. Denis, S. L. Hir, F. Quentel, C. Elléouet, T. Montier, J-M. Rueff, J-Y. Salaün, J-P. Haelters, G. B. Hix, P. Lehn and P-A. Jaffrès, *New J. Chem.*, 2011, **35**, 1000-1003.

S11 C. Y. Sun, C. Qin, C. G. Wang, Z. M. Su, S. Wang, X. L. Wang, G. S. Yang, K. Z. Shao, Y. Q. Lan and E. B. Wang, *Adv. Mater.*, 2011, **23**, 5629-5632.

S12 F. Ke, Y. P. Yuan, L. G. Qiu, Y. H. Shen, A. J. Xie, J. F. Zhu, X. Y. Tian and L. D. Zhang, *J. Mater. Chem.*, 2011, **21**, 3843-3848.

S13 Z. Y. Gu, Y. J. Chen, J. Q. Jiang and X. P. Yan, *Chem. Commun.*, 2011, **47**, 4787-4789.

S14 (a) P. Horcajada, T. Chalati, C. Serre, B. Gillet, C. Sebrie, T. Baati, J. F. Eubank, D. Heurtaux, P. Clayette, C. Kreuz, J. S. Chang, Y. K. Hwang, V. Marsaud, P. N. Bories, L. Cynober, S. Gil, G. Férey, P. Couvreur and R. Gref, *Nat. Mater.*, 2010, **9**, 172-178. (b) T. Chalati, P. Horcajada, P. Couvreur, C. Serre, M. Ben Yahia, G. Maurin and R. Gref, *Nanomedicine (Lond)*, 2011, **6**, 1683-1695.S15 H.N. Wang, X. Meng, G. S. Yang, X. L. Wang, K. Z. Shao, Z. M. Su and C. G. Wang, *Chem. Commun.*, 2011, **47**, 7128-7130.

S16 R. Ananthoji, J. F. Eubank, F. Nouar, H. Mouttaki, M. Eddaoudi and J. P. Harmon, *J. Mater. Chem.*, 2011, **21**, 9587-9594.

S17 C. Gaudin, D. Cunha, E. Ivanoff, P. Horcajadab, G. Chevéc, A. Yasric, O. Logetc, C. Serreb and G. Maurina, *Micropor. Mesopor. Mat.*, 2012, **157**, 124-130.

S18 (a) M. Eddaoudi, H.L. Li and O. M. Yaghi, *J. Am. Chem. Soc.*, 2000, **122**, 1391-1397. (b) M. O. Rodrigues, M. V. de Paula, K. A. Wanderley, I. B. Vasconcelos, Jr. Alves and T. A. Soares, *Int. J. Quantum. Chem.*, 2012, **112**, 3346-3355.

S19 J. S. Qin, Y. Q. Lan, D. Y. Du, W. L. Li, J. P. Zhang, S. L. Li, Z. M. Su, X. L. Wang, Q. Xu, K. Z. Shao and Y. Q. Lan, *Chem. Sci.*, 2012, **3**, 2114-2118.

S20 (a) A. Vishnyakov, P. I. Ravikovitch, A. V. Neimark, M. Bulow, Q. M. Wang, *Nano Letters*, 2003, **6**, 713-718. (b) F.R. Lucena, L.C. de Araújo, M. D. Rodrigues, T. G. da Silva, V. R. Pereira, G. C. Militão, D. A. Fontes, P. J. Rolim-Neto, F. F. da Silva

and S. C. Nascimento, *Biomed. Pharmacother.*, 2013, **67**, 707-713.
S21 (a) S. Rojas, P. S. Wheatley, E. Quartapelle-Procopio, B. Gilc, B. Marszalekc, R. E. Morris and E. Barea , *CrystEngComm.*, 2013, **15**, 9364-9367. (b) D. Cattaneo, S.J. Warrender, M.J. Duncan, C.J. Kelsall, M.K. Doherty, P.D. Whitfield, I. L. Megson, R. E. Morris, *RSC Adv.*, 2016, **6**, 14059-14067.S22 D. Cunha, M. Ben Yahia, S. Hall, S. R. Miller, H. Chevreau, E. Elkaïm, G. Maurin, P. Horcajada and C. Serre, *Chem. Mater.*, 2013, **25**, 2767-2776.
S23 Y. L. Hu, C. Y. Song, J. Liao, Z. L. Huang and G. K. Li, *J. Chromatogr. A*, 2013, **1294**, 17-24.
S24 Q. Hu, J. C. Yu, M. Liu, A. P. Liu, Z. S. Dou and Y. Yang, *J. Med. Chem.*, 2014, **57**, 5679-5685.
S25 S. Devautour-Vinot, S. Diaby, D. D. Cunha, C. Serre, P. Horcajada and G. Maurin, *J. Phys. Chem. C*, 2014, **118**, 1983-1989.
S26 T. Kundu, S. Mitra, P. Patra, A. Goswami, D. Díaz and R. Banerjee, *Chem. – Eur. J.*, 2014, **20**, 10514-10518.
S27 C. B. He, K. D. Lu, D. M. Liu and W. B. Lin, *J. Am. Chem. Soc.*, 2014, **136**, 5181-5184.
S28 M. R. di Nunzio, V. Agostoni, B. Cohen, R. Gref and A. A. Douhal, *J. Med. Chem.*, 2014, **57**, 411-420.
S29 M. Tsotsalas, J. Liu, B. Tettmann, S. Grosjean, A. Shahnas, Z. Wang, C. Azucena, M. Addicoat, T. Heine, J. Lahann, J. Overhage, S. Bräse, H. Gliemann and C. Wöll, *J. Am. Chem. Soc.*, 2014, **136**, 8-11.
S30 C. Zlotea, R. Campesi, F. Cuevas, E. Leroy, P. Dibandjo, C. Volkringer, T. Loiseau, G. Férey and M. Latroche, *J. Am. Chem. Soc.*, 2010, **132**, 2991-2997.
S31 V. Agostoni, T. Chalati, P. Horcajada, H. Willaime, R. Anand, N. Semiramoth, T. Baati, S. Hall, G. Maurin, H. Chacun, K. Bouchemal, C. Martineau, F. Taulelle, P. Couvreur, C. Rogez-Kreuz, P. Clayette, S. Monti, C. Serre and R. Gref, *Adv. Healthc. Mater.*, 2013, **2**, 1630-1637.
S32 V. Agostoni, R. Anand, S. Monti, S. Hall, G. Maurin, P. Horcajada, C. Serre, K. Bouchemal and R. Gref, *J. Mater. Chem.* B, 2013, **1**, 4231-4242.
S33 R. Anand, F. Borghi, F. Manoli, I. Manet, V. Agostoni, P. Reschiglian, R. Gref and S. Monti, *J. Phys. Chem.* B, 2014, **118**, 8532-8539.
S34 V. Rodriguez-Ruiz, A. Maksimenko, R. Anand, S. Monti, V. Agostoni, P. Couvreur, M. Lampropoulou, K. Yannakopoulou and R. Gref, *J. Drug Target.*, 2015, **23**, 759-767.
S35 A. Pardakhty, M. Ranjbar, *Nanomed. J.*, 2016, **3**: 248-252.